Gene Therapy Bio-factory: Mathematical Modeling of the Human Eye Pharmacokinetics

Lucia Carichino, Giovanna Guidoboni, Viral Kansara, Thomas Ciulla, and Alon Harris

1 Introduction

Neovascular age-related macular degeneration (nAMD) is the leading cause of irreversible central blindness in the industrialized world [1–3]. The retina is the innermost light-sensitive layer of the eye (see Fig. 1). The retina receives images refracted through the cornea and lens, converting them into electric signals that are transmitted to the brain via the optic nerve. Most of the central vision is processed by the macula, which is a narrow region of the retina directly posterior to the lens. The retinal pigment epithelium (RPE), Bruch's membrane and choroid are the tissue layers directly opposed and peripheral to the retina (see Fig. 1); the choroid consists mostly of blood vessels that transport oxygen and nutrients to the ocular tissue. The retina and the choroid are separated by the Bruch's membrane [4]. In nAMD, abnormal blood vessel growth occurs from the choriocapillaris, a layer of capillaries in the choroid situated immediately below the Bruch's membrane, under the macula, resulting in choroidal neovascularization. These newly formed blood vessels leak blood, lipids, and serum into the retinal layers causing the macula to bulge or elevate from its normal position, distorting central vision [4].

L. Carichino (✉)
School of Mathematics and Statistics, Rochester Institute of Technology, Rochester, NY, USA
e-mail: lcsma1@rit.edu

G. Guidoboni
College of Engineering and Computing Professor, Electrical and Computer Engineering, The University of Maine, Orono, ME, USA

V. Kansara · T. Ciulla
Clearside Biomedical Inc., Alpharetta, GA, USA

A. Harris
Icahn School of Medicine at Mount Sinai, New York, NY, USA

© The Author(s), under exclusive license to Springer Nature Switzerland AG 2024

D. Wanduku et al. (eds.), *Applied Mathematical Analysis and Computations II*,
Springer Proceedings in Mathematics & Statistics 472,
https://doi.org/10.1007/978-3-031-69710-4_3

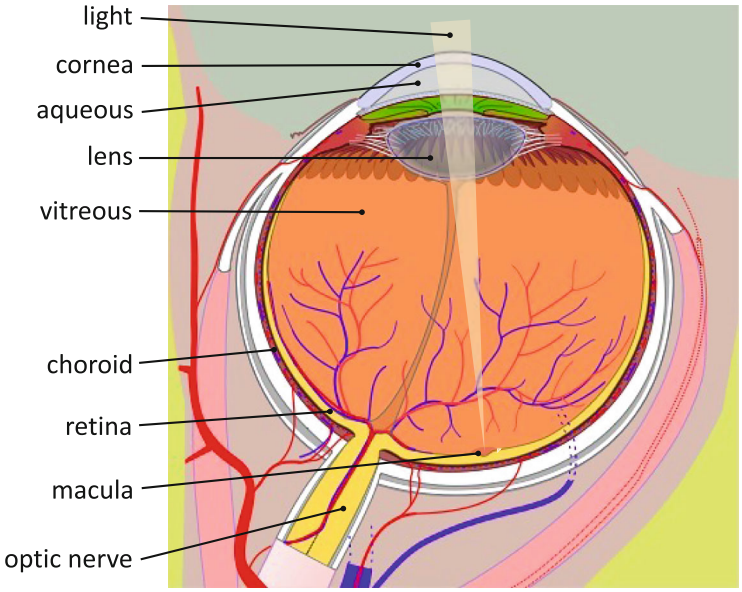

Fig. 1 Anatomy of the right human eye, adapted from [5]

The risk factors and pathogenesis of nAMD are complex and not fully understood. Of note, the vascular endothelial growth factor (VEGF) signaling pathway has been shown to be centrally involved in the 10–15% of AMD diagnoses classified as the neovascular type (nAMD). In this pathway, VEGF signaling ligands bind to different VEGF receptors to activate cellular processes that promote vascular permeability and growth of new vasculature [6, 7]. It is this pathway that is targeted in current nAMD therapies, often in the form of intravitreal injections of anti-VEGF drugs to repress the growth of the choroidal neovascularization [8].

The current standard of care anti-VEGF therapeutics for the treatment of nAMD targets VEGF-A protein [9], and require frequent injections to maintain sustained chronic VEGF suppression, due to limited durability of these therapies. This dosing regimen creates significant treatment burden on patients, caregivers and physicians, consequently resulting in missed treatment visits, and lack of sustained anti-VEGF levels in the eye [10]. In fact, the therapeutic benefit of these drugs is suboptimal [11, 12]. The visual acuity results from randomized clinical studies revealed that despite fixed frequent (i.e., up to monthly) protocol mandated intravitreal injection over 1 year, 20% of patients lose visual acuity, and approximately 50% do not achieve clinically meaningful visual acuity [13–15]. Recent large "real-world" retrospective studies of nAMD further underscore the difficulty in adhering to the dosing regimens [16–20].

Gene therapy based long-lasting production of anti-VEGF proteins in the eye is currently under clinical investigation [21], and may address some of the limitations of the current anti-VEGF therapies by eliminating the need for frequent injections. Gene therapy-based bio-factory approach delivers necessary genetic information to the ocular cells that enables ocular cells to continuously produce and release anti-VEGF proteins using existing protein-making machinery in these cells. Moreover, this localized production and release of anti-VEGF proteins may have beneficial local distribution characteristics compared to existing intravitreal administration. When administered to the vitreous humor via injections, the anti-VEGF drug must first diffuse through the vitreous humor, retina and the Bruch's membrane before reaching the target choroidal neovascularization. Instead, using the gene therapy bio-factory approach, the cells in the target tissues, such as retina, retinal pigment epithelium (RPE), and choroid, would produce the anti-VEGF proteins targeting the adjacent choroidal neovasculature.

Following drug injections (gene therapy or anti-VEGF drug), levels of anti-VEGF in the aqueous humor can be measured in the clinic. This is more challenging, however, for other posterior ocular compartments such as the retina and choroid due to the invasive nature of such sampling. To address this limitation, mathematical models have been proposed to estimate target tissue drug levels that cannot be assessed directly.

Various mathematical models have been developed to study ocular pharmacokinetics after intraocular injections. In some models, the ocular compartments are described at the continuum level in two or three spatial dimensions [22–24], while other models adopt a less detailed approach based on lumped compartmental models, where the drug concentration is assumed to be uniform in space within each compartment [25–27]. Xu et al. [25] developed a population based approach to estimate the anti-VEGF drug (ranibizumab) concentration in humans in the vitreous humor and in the serum using experimental data of serum concentrations from AMD patients included in clinical trials. Hutton-Smith et al. [27] proposed a three-compartment (retina, vitreous humor, aqueous humor) pharmacokinetic model to estimate intraocular permeabilities in rabbits and study the effect of drug molecule size.

Here, we adapt the model by Hutton-Smith et al. [27] and calibrate it with human data to simulate the pharmacokinetics of anti-VEGF proteins in the human eye delivered by intravitreal injection or produced via the gene therapy bio-factory approach. The model is used to leverage the clinically measured levels of anti-VEGF in the aqueous humor in order to estimate the anti-VEGF production rate in the retina using the gene therapy bio-factory approach. Next, the model is used to estimate the protein levels in the vitreous humor and retina starting from clinically measured anti-VEGF protein levels in the aqueous humor. The modeling results have important applications in the development of novel therapies, improving the understanding and prediction of dosage, durability, and dosing interval.

2 Methods

2.1 Mathematical Model

We started from a model based on ordinary differential equations developed by Hutton-Smith et al. [27], which includes three ocular compartments: the aqueous humor (AQ), the vitreous humor (VIT) and the retina (RET), see Fig. 2. In this work, we adapted the three compartmental model to human pharmacokinetics and we modified it to account for the two different drug delivery systems considered in this work, i.e. intraocular injection and gene therapy.

The model depicted in Fig. 2 can be formulated as a system of ordinary differential equations in terms of the drug concentrations in each of the three model compartments, denoted by $C_{AQ}(t)$, $C_{VIT}(t)$ and $C_{RET}(t)$. The concentrations are assumed to be spatially constant in each compartment and to vary with time t. Given the initial conditions $C_{AQ}(0)$, $C_{VIT}(0)$ and $C_{RET}(0)$, we solve

$$\frac{dC_{RET}}{dt} = -\frac{S}{V_{RET}} p_{ILM} \left(C_{RET} - C_{VIT}\right) - \frac{S}{V_{RET}} p_{RPE} C_{RET} + \frac{r}{V_{RET}}, \tag{1}$$

$$\frac{dC_{VIT}}{dt} = -\frac{S}{V_{VIT}} p_{ILM} \left(C_{VIT} - C_{RET}\right) - k_{EL} C_{VIT}, \tag{2}$$

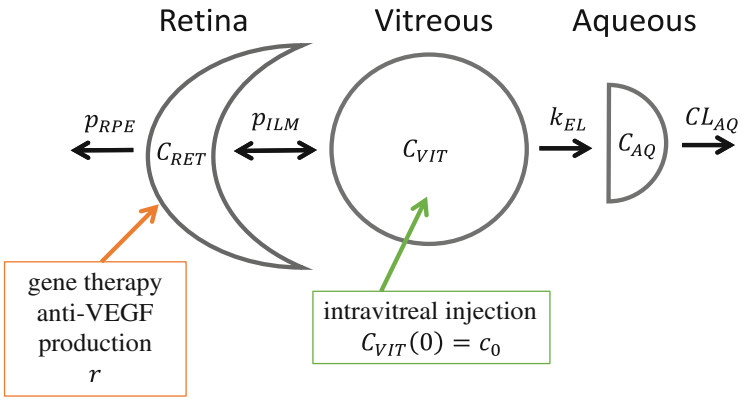

Fig. 2 Sketch of the three compartment model: aqueous humor (AQ), vitreous humor (VIT) and retina (RET). The black arrows represent the pathways between, in and out each compartment, and the corresponding model parameters. C_i is the drug concentration in the i-th compartment, for $i = RET, VIT, AQ$. The model can simulate the dynamics after an intravitreal injection by assuming a non-zero initial condition in the vitreous humor, i.e. $C_{VIT}(0) = c_0$, or can simulate the dynamics after a gene therapy treatment by assuming a non-zero anti-VEGF production rate $r = r_0$ in the retina

$$\frac{dC_{AQ}}{dt} = k_{EL}\frac{V_{VIT}}{V_{AQ}}C_{VIT} - \frac{CL_{AQ}}{V_{AQ}}C_{AQ}. \tag{3}$$

Here, V_i is the volume of the i-th compartment, for $i = RET, VIT, AQ$. p_{ILM} is the permeability of the inner limiting membrane (ILM), located between the retina and the vitreous humor, p_{RPE} is the permeability of the retinal pigment epithelium (RPE), located between the retina and the choroid (see Fig. 1). k_{EL} is the elimination rate from the vitreous humor to the aqueous humor, CL_{AQ} is the clearance from the aqueous humor, and r is the gene therapy anti-VEGF production rate in the retina. The surface areas of the RPE and ILM are assumed to be equal to each other and equal to S [27]. This assumption is justified by the fact that the thickness of the retina is two orders of magnitude smaller than the radius of the vitreous humor chamber [23, 27]. For more details on the model derivation and on the definition of the model parameters we refer to Appendix A and Hutton-Smith et al. [27].

The model (1)–(3) can be used to simulate both scenarios of intravitreal injection and gene therapy in the following way. For intravitreal injections, C_i for $i = RET$, VIT, AQ, represent the drug concentration, e.g. ranibizumab, in each compartment, and can be simulated with the model by setting the initial conditions

$$C_{AQ}(0) = C_{RET}(0) = 0, C_{VIT}(0) = c_0 \text{ and } r = 0, \tag{4}$$

where c_0 is the concentration of the drug injected in the vitreous humor. For gene therapy, C_i for $i = RET$, VIT, AQ represent the concentration of anti-VEGF protein (produced by the retina) in each compartment, and can be simulated with the model by setting the initial conditions

$$C_{AQ}(0) = C_{RET}(0) = C_{VIT}(0) = 0 \text{ and } r = r_{0,} \tag{5}$$

where r_0 is the constant anti-VEGF production rate in the retina.

Let's consider now the steady state solution, i.e. the long term behavior in time of the system (1)–(3). Setting the time derivatives equal to zero in (1)–(3), we can compute the steady state values of the concentrations in the various model compartment as

$$\overline{C_{RET}} = \frac{r\,(p_{ILM}S + k_{EL}V_{VIT})}{S\,(p_{ILM}p_{RPE}S + k_{EL}V_{VIT}\,(p_{ILM} + p_{RPE}))}, \tag{6}$$

$$\overline{C_{VIT}} = \frac{r\;p_{ILM}}{(p_{ILM}p_{RPE}S + k_{EL}V_{VIT}\,(p_{ILM} + p_{RPE}))}, \tag{7}$$

$$\overline{C_{AQ}} = \frac{r\,(p_{ILM}\,k_{EL}V_{VIT})}{CL_{AQ}\,(p_{ILM}p_{RPE}S + k_{EL}V_{VIT}\,(p_{ILM} + p_{RPE}))}, \tag{8}$$

where the overbar indicates the steady state solution. Note that, in the intravitreal injection scenario, we have that $r = 0$, thereby implying that the steady state solution is $\overline{C_{AQ}} = \overline{C_{RET}} = \overline{C_{VIT}} = 0$. In other words, after a long time from the intravitreal injections, the drug is totally washed out from the eye. Conversely, in the gene therapy scenario, we have that $r = r_0$ and the model reaches a steady state that consists of a non-zero equilibrium $\overline{C_{AQ}}(r_0), \overline{C_{RET}}(r_0), \overline{C_{VIT}}(r_0) > 0$. In other words, after a long time from the beginning of the gene therapy treatment, the production of anti-VEGF in the retina is capable of sustaining a constant concentration of anti-VEGF protein in each compartment. Note that Eqs. (6)–(8) are derived under the assumption that the retinal production rate r is known. However, in the experimental setting, this is not the case, as r cannot be measured directly; the anti-VEGF concentration in the aqueous humor, on the other hand, can be accessed and measured. Hence, in the gene therapy bio-factory approach, if we assume that the steady state concentration in the aqueous humor $\overline{C_{AQ}}$ is known (from experiments), we can rewrite Eqs. (6)–(8) to find the retinal production rate $r = r_0$ (that would yield such concentration in the aqueous humor) and the corresponding concentrations in vitreous humor and retina as follows

$$r_0 = \frac{\overline{C_{AQ}}\, CL_{AQ}\,(p_{ILM} p_{RPE} S + k_{EL} V_{VIT}\,(p_{ILM} + p_{RPE}))}{(p_{ILM}\, k_{EL} V_{VIT})}, \tag{9}$$

$$\overline{C_{RET}} = \frac{\overline{C_{AQ}}\, CL_{AQ}\,(p_{ILM} S + k_{EL} V_{VIT})}{S\,(p_{ILM}\, k_{EL} V_{VIT})}, \tag{10}$$

$$\overline{C_{VIT}} = \frac{\overline{C_{AQ}}\, CL_{AQ}}{k_{EL} V_{VIT}}. \tag{11}$$

2.2 Model Parameters

The values of the model parameters are reported in Table 1. Geometrical ocular parameters for humans, i.e. S and V_i for $i = RET, VIT, AQ$, are estimated from existing literature. In particular, we assume $V_{\mathrm{VIT}} = 4.85$ ml and $V_{\mathrm{AQ}} = 0.24$ ml [23, 28]. We estimated S and V_{RET} by assuming that the vitreous humor chamber is a sphere of volume V_{VIT}, the retinal thickness is 0.02 cm [23], and the human ocular geometrical structure is as reported in [23]. For more details on the derivation of S and V_{RET} we refer to the Supporting Information of [27]. The value of the clearance from the aqueous humor CL_{AQ} is based on experimental findings, assuming that CL_{AQ} is equivalent to the mean aqueous humor flow rate in humans of 2.75 μl/min [29].

To estimate the elimination rate k_{EL} from the vitreous humor to the aqueous humor and the permeabilities coefficients p_{ILM} and p_{RPE}, we used experimental values of aqueous humor concentrations in humans after intravitreal injection reported

Table 1 Parameters used for model simulations

Parameter	Value	Reference
Volume vitreous humor compartment, V_{VIT}	4.85 ml	[23, 28]
Volume aqueous humor compartment, V_{AQ}	0.24 ml	[23, 28]
Volume retina compartment, V_{RET}	0.24 ml	[a]
Surface area, S	10.80 cm^2	[a]
Ratio p_{RPE}/p_{ILM}	1.38	[27]
RPE permeability, p_{RPE}	1.72×10^{-8} cm/s	[b]
Elimination rate from vitreous to aqueous, k_{EL}	9.58×10^{-2} 1/day	[b]
Clearance from the aqueous humor, CL_{AQ}	2.75 μl/min	[29]

[a]Estimated following [27]
[b]Estimated fitting experimental data

by Krohne et al. [30]. Krohne et al. measured concentrations of ranibizumab (anti-VEGF drug) in aqueous humor samples extracted from 18 patients during cataract surgery 1–37 days after receiving a single intravitreal injection of 0.5 mg of ranibizumab. The mean results of triplicate measurements from [30] are reported in Fig. 3 (center and right panels), where the squares represent data pertaining to nAMD patients while the circles represent data pertaining to patients with diabetic macular edema and central or branch retinal vein occlusion with secondary macular edema. For the parameter estimation, we use all the data reported in [30] and normalize them with respect to the initial peak concentration of 56.1 μg/ml reported in [30]. The model results are normalized with respect to the maximum value of aqueous humor concentration attained by the model. We determine the parameters k_{EL}, p_{ILM} and p_{RPE}, similarly to [27], using the MATLAB solver *lsqnonlin* that minimizes the relative mean-square error between the normalized logarithmic values of model results and the experimental data [27, 31]. As initial guess values for the *lsqnonlin* we used the values k_{EL}, p_{ILM} and p_{RPE} estimated for rabbits in [27]. Additionally, in the minimization process, we assumed the ratio p_{RPE}/p_{ILM} in humans to be the same as the ranibizumab (Fab) ratio reported in [27] for rabbits, see Table 1.

Figure 3 shows model predicted concentrations (left) in each compartment computed using the parameters values reported in Table 1. The comparison between normalized experimentally measured (circles and squares) [30] and model predicted (solid line) aqueous humor concentrations are reported in arithmetic scale (center) and logarithmic scale (right). The model predictions are obtained under initial conditions (4) with $c_0 = 0.5/(V_{\mathrm{VIT}} + 0.05)$ mg/ml, assuming that the intravitreal injection has a volume of 0.05 ml [32]. After parameter estimation, the model predicts a drug elimination half-life in the aqueous humor of 7.23 days, in agreement with [30], and a concertation in the vitreous humor C_{VIT} in the range $0 - 120$ μg/ml, consistently with the results obtained with the mathematical model developed by Xu et al. [25].

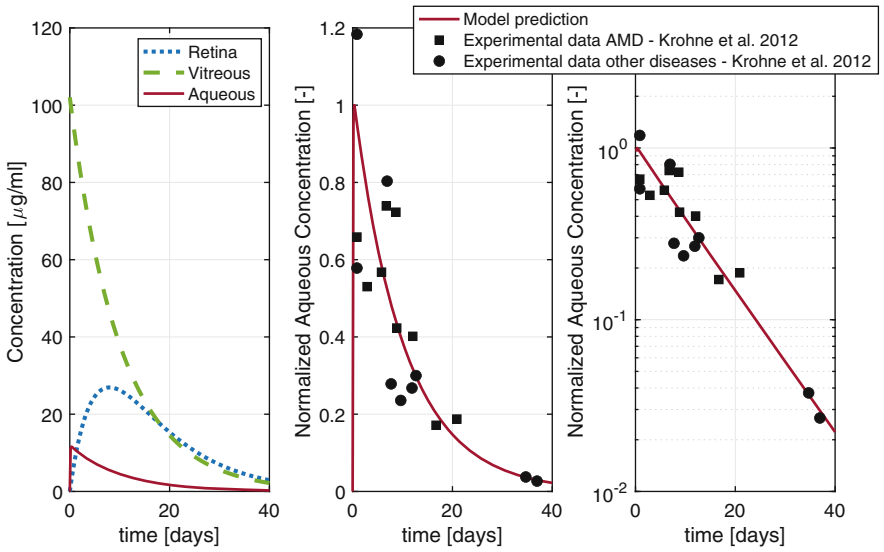

Fig. 3 Model predictions after a single intravitreal injection of 0.5 mg of ranibizumab in humans. Model predictions (left) for drug concentrations in each compartment. Comparison between experimentally measured (circles and squares) [30] and model predicted (solid line) normalized aqueous humor concentrations in arithmetic scale (center) and semi-logarithmic scale (right). The squares represent data pertaining to age-related macular degeneration (AMD) patients, while the circles represent data pertaining to patients with diabetic macular edema and central or branch retinal vein occlusion with secondary macular edema

3 Results

The model described in Sect. 2 is used to leverage data of drug concentration in the aqueous humor from a gene therapy clinical trial to estimate the retinal production rate during gene therapy treatment, as detailed in Sect. 3.1. In Sect. 3.2, we compared the model predicted ocular pharmacokinetics profiles for the monthly intravitreal injections treatment and the gene therapy treatment.

3.1 Estimated Gene-Therapy Retinal Production Rate

To estimate the retinal production rate during gene therapy treatment, we refer to publicly disclosed information of anti-VEGF concentration levels in the aqueous humor from a nAMD gene therapy clinical trial [33–35]. The clinical trial included five different cohorts, that received five different doses of the gene therapy treatment delivered subretinally, between the RPE cells and the retinal photoreceptors. After a month from the gene therapy treatment, a patient in the clinical trial could receive intravitreal injections of anti-VEGF drugs, if necessary. For this reason, we

Table 2 Clinical data of anti-VEGF concentration in the aqueous humor 1 month after treatment, for the five cohorts included in the clinical trial [33–35], mean and standard deviation. Corresponding mean and standard deviation of anti-VEGF retinal production rates r_0 estimated using the mathematical model

Cohorts	Anti-VEGF concentration in the aqueous humor	Retinal anti-VEGF production rate, r_0
Cohort 1	2.5(±2.1) ng/ml	$0.017(\pm 0.014) \times 10^3$ ng/day
Cohort 2	12.8(±5.7) ng/ml	$0.089(\pm 0.040) \times 10^3$ ng/day
Cohort 3	160.2(±87.8) ng/ml	$1.116(\pm 0.612) \times 10^3$ ng/day
Cohort 4	249.4(±49.6) ng/ml	$1.737(\pm 0.345) \times 10^3$ ng/day
Cohort 5	376.0(±69.7) ng/ml	$2.619(\pm 0.486) \times 10^3$ ng/day

used the anti-VEGF level in the aqueous humor reported a month after the gene therapy treatment, for each cohort, before any patient would receive any additional treatment [33]. The mean and standard deviation of the anti-VEGF levels in the aqueous humor in the five cohorts, a month after the gene therapy treatment, are reported in Table 2. We assumed that the steady state concentrations achieved by the model in the aqueous humor $\overline{C_{AQ}}$ in eqs. Eqs. (9)–(11) to be equal to the anti-VEGF concentrations reported in Table 2. Next, we solved Eqs. (9)–(11) with the parameters values reported in Table 1 to compute the retinal production rates and the concentrations in the retinal and vitreous humor compartments for the five cohorts.

Table 2 reports the model predictions of retinal production rate r_0 for the five $\overline{C_{AQ}}$ levels considered. For each cohort, mean values and standard deviation of the predictions are reported. Figure 4 shows the steady state anti-VEGF concentrations in the vitreous humor $\overline{C_{VIT}}$ and in the retina $\overline{C_{RET}}$ for the five $\overline{C_{AQ}}$ levels considered. The results suggest that $\overline{C_{AQ}} > 160$ ng/ml (cohorts 3–5) correspond to $\overline{C_{RET}} > 3 \times 10^4$ ng/ml and $r_0 > 1 \times 10^3$ ng/day, while $\overline{C_{AQ}} < 160$ ng/ml (cohorts 1–2) correspond to $\overline{C_{RET}} < 0.3 \times 10^4$ and $r_0 < 0.1 \times 10^3$ ng/day. Moreover, since the model is linear, from Eqs. (9)–(11), changes in $\overline{C_{AQ}}$ would have a constant effect on the model predictions of Eqs. (9)–(11). In particular, the model suggests that a $\overline{C_{AQ}}$ increase of 1 ng/ml corresponds to a $\overline{C_{VIT}}$ increase of 8.5 ng/ml and a $\overline{C_{RET}}$ increase of 187 ng/ml, corresponding to an increase of 7.0 ng/day in r_0.

3.2 Intravitreal Injections vs. Gene Therapy Pharmacokinetics

We compared the model predicted ocular pharmacokinetics of anti-VEGF proteins in the human eye delivered by intravitreal injection or produced via the gene therapy bio-factory approach delivered subretinally. For intravitreal injections, we solved Eqs. (1)–(3) with condition (4) and consider monthly injections of 0.5mg (assuming that each intravitreal injection has a volume of 0.05 ml [32]). For gene therapy, we solved Eqs. (1)–(3) and condition (5) with the five different retina production rates r_0 estimated in Sect. 3.1 and reported in Table 2 (one r_0 for each cohort included

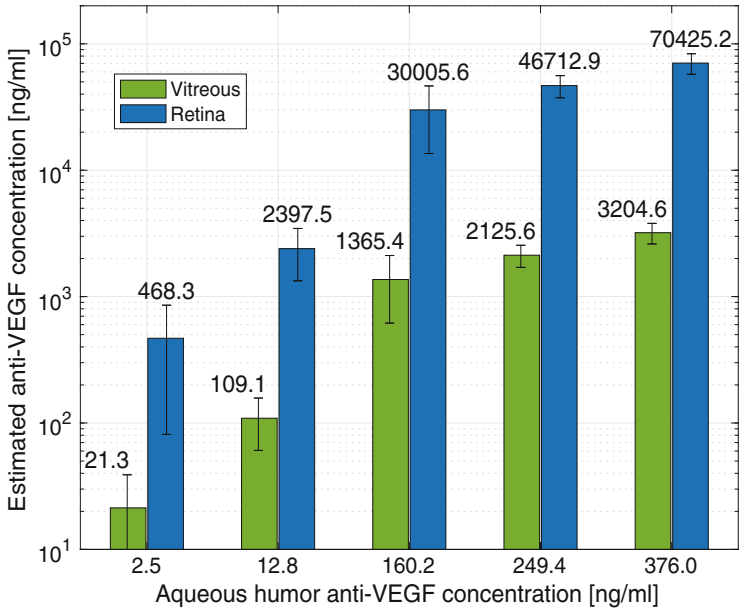

Fig. 4 Model predictions of anti-VEGF concentration in the vitreous humor and in the retina based on the drug concentration in the aqueous humor reported in the five different cohorts of the clinical trial in [33–35] 1 month after treatment

in the clinical trial [33–35]). In both cases, we solved (1)–(3) using the method of matrix exponential, see Appendix B for more details.

Figure 5 shows the comparison of the model predicted concentrations in retina (left), vitreous humor (center) and aqueous humor (right) compartments for the monthly intravitreal injection scenario (dashed black curve) and the gene therapy scenario (colored solid curves) in semi-logarithmic scale. For intravitreal injections, the simulation results show how drug concentrations in each compartment decrease exponentially between injections and increase again when a new injection is administered. For gene therapy, the model predicts that the anti-VEGF concentration in each compartment increases with time and reaches a steady state. In the vitreous humor and aqueous humor, the model predicts that drug levels after intravitreal injections are significantly higher than anti-VEGF levels after a gene therapy treatment. However, in the retina, the concentrations of anti-VEGF after a gene therapy treatment with retinal production rates r_0 larger than 1×10^3 ng/day (cohorts 3–5) are higher or equal to the drug concentrations after intravitreal injections. This is not the case, however, when values of r_0 less than 0.1×10^3 ng/day are considered (cohorts 1–2).

In-vitro, in a human umbilical vein endothelial cell, when ranibizumab concentrations was greater than 1.29 nM, or equivalently 61.92 ng/ml (assuming ranibizumab molecular weight of 48 kDa [36]), maximal inhibition of VEGF-A

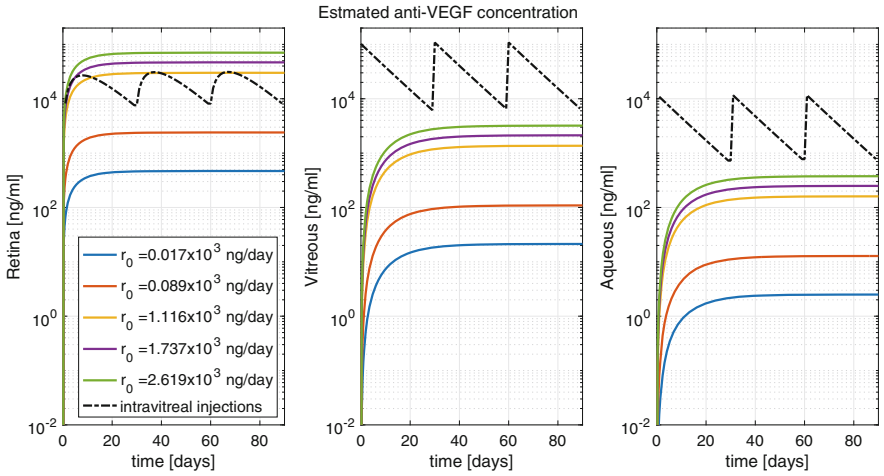

Fig. 5 Comparison of model predicted concentrations in the retina (left), vitreous humor (center) and aqueous humor (right) compartments for gene therapy (colored solid curves) vs monthly intravitreal injections (dashed black curve) in semi-logarithmic scale. The gene therapy retinal production rates r_0 considered are based on the five different cohorts of the clinical trial in [33–35]

proliferation was observed [37]. Our results show that retinal concentrations are constantly higher than the threshold of 61.92 ng/ml after intravitreal injections. In the gene therapy scenario, the estimated retinal concentrations levels surpass the threshold at most one day after treatment for all the five cohorts considered.

4 Discussion and Conclusions

In this work, we adapted a compartmental model of pharmacokinetics in rabbits to study the behavior of drugs delivered to the human eye via intravitreal injection or gene therapy. We have estimated permeabilities and elimination rates in the human eye by fitting the model to experimental data. After parameter fitting, the model-predicted drug concertation in the vitreous humor obtained in the case of intravitreal injection was found to be consistent with published literature [25].

Next, we extended the model to study the gene therapy bio-factory approach. We used publicly disclosed data of anti-VEGF concentration levels in the aqueous humor of patients undergoing a nAMD gene therapy clinical trial, a month after the treatment. Using these data, we have estimated the corresponding retinal anti-VEGF productions rate and the concentrations in the remaining ocular compartment. In particular, in cohorts 3–5, with an aqueous humor concentration greater than 160 ng/ml a month after the treatment, the model estimated a retinal production rate $r_0 > 1 \times 10^3$ ng/day.

Finally, we compared the anti-VEGF concentrations in each ocular compartment delivered via monthly intravitreal injections or produced via the gene therapy bio-factory approach. In cohorts 3–5, the model predicted gene therapy anti-VEGF concentrations in the retina similar or higher to the drug concentrations after intravitreal injections, see Fig. 5. It is important to note that, among the three compartments considered in this work, the retina is the one physically closest to the choroidal neovascularization, which is the ultimate target of the anti-VEGF protein. Hence, in cohorts 3–5, the model suggests that the gene therapy treatment is at least as efficient as the intravitreal injections in targeting choroidal neovascularization. These results are consistent with the findings of the nAMD gene therapy clinical trial presented in [35]. The patients in cohorts 3–5, 2 years after the beginning of the trial, exhibited stable or improved ocular anatomy, measured via central retinal thickness, and a $58 - 85\%$ reduction in the number of intravitreal injections needed after the gene therapy treatment [35].

The model also suggests that a similar concentration in the retina would correspond to different concentrations in the aqueous humor depending on whether the drug was delivered via intravitreal injections or gene therapy, see Fig. 5. In particular, for monthly intravitreal injections, a concentration of 3×10^4 ng/ml in the retina would correspond to a concentration of approximately 6×10^3 ng/ml in the aqueous humor. However, after a gene therapy treatment, a concentration of 3×10^4 ng/ml in the retina would correspond to a concentration of approximately 1.5×10^2 ng/ml in the aqueous humor. This is due to a fundamental difference in the driving mechanisms behind the two treatments. During intravitreal injection, the drug is administered directly in the vitreous humor, from which it will diffuse into the aqueous humor. In subretinal administration of gene therapy, the anti-VEGF is produced within the retina and it will need to pass through the ILM and diffuse through the vitreous humor before reaching the aqueous humor. This dynamic would likely also apply to suprachoroidal administration of gene therapy, which may result in meaningful local levels of therapeutic protein, which are significantly lower in the aqueous humor, several compartments distal. Since concentrations in the aqueous humor can be measured in the clinic, it is important to take into account the treatment delivery system when interpreting the physiological implications of such measurements.

The modeling effort presented in this work has limitations. First, we focused on anti-VEGF production via retinal cells in this work, however ocular compartments other than retina such as the RPE and the choroid may also play a role. The RPE and the choroid may contribute to the anti-VEGF ocular production after the gene therapy treatment [38]. More complex models incorporating these compartments, can be further investigated in future work. Additionally, the gene therapy treatment considered in this manuscript is administered in the subretinal space, between the RPE cells and the retinal photoreceptors, and it would be interesting to study how the dynamics in this additional compartment would change the ocular pharmacokinetics predicted by the model. A further model limitation is related to the drug elimination pathways that are currently accounted for. In the model the main drug elimination pathways are the aqueous humor outflow, via the trabecular meshwork, and the

absorption into the choroid, neglecting more complex human ocular elimination pathways, such as the uveoscleral outflow, and other pathways unique to subretinal administered gene therapy. Importantly, gene therapy remains a nascent procedure and assumptions of constant production of anti-VEGF r may not hold true.

Despite its limitations, this modeling effort may enable to estimate therapeutic protein levels in ocular compartments that are challenging to access in a clinical setting. In the future, precision medicine aided by these mathematical models may be used to enhance the understanding and prediction of key pharmacokinetic parameters such as dosage, durability and dosing interval. Further study is warranted.

Acknowledgments The authors would like to thank Jennifer Sebell for the help in reviewing the literature and Simone Cassani for the useful discussions. The present work has been partially supported by the National Science Foundation grants DMS 2108711/2108665 and DMS 1853222/2021192, and by the National Eye Institute of the National Institutes of Health under Award Number R01EY034718. The content is solely the responsibility of the authors and does not necessarily represent the official views of the National Institutes of Health.

Appendices

Appendix A: Model Derivation

We report here additional details on the derivation of the model presented in [27] and described by Eqs. (1)–(3). In the model, three ocular compartments are considered: the aqueous humor, the vitreous humor and the retina. For each compartment, the mass conservation law is used to describe the dynamics of the amount of drug at time t as follows

$$\frac{dm_{RET}}{dt} = -J_{ILM} - J_{RPE} + r, \tag{12}$$

$$\frac{dm_{VIT}}{dt} = J_{ILM} - J_{EL}, \tag{13}$$

$$\frac{dm_{AQ}}{dt} = J_{EL} - J_{CL}\ . \tag{14}$$

Here, m_i is the amount of drug in the i-th compartment, for $i = RET, VIT, AQ,$ and r is the gene therapy anti-VEGF production rate in the retina. Note that, the mass m_i and the concentration C_i of the drug in each compartment are proportional to each other via $m_i = C_i V_i$, for $i = RET, VIT, AQ,$ where $\mathrm{V_i}$ is the volume of the i-th compartment.

In Eqs. (12)–(14), J represent the fluxes in between, in and/or out each compartment. In particular, J_{ILM} is the flux between the retina and the vitreous

humor through the inner limiting membrane (ILM). The flux J_{ILM} is modeled using a modified version of Fick's law as

$$J_{ILM} = S\, p_{ILM} \left(\frac{m_{RET}}{V_{RET}} - \frac{m_{VIT}}{V_{VIT}} \right) = S\, p_{ILM} \left(C_{RET} - C_{VIT} \right). \tag{15}$$

Fick's law assumes that the drug molecules move from the compartment with higher drug concentration to the compartment with lower drug concentration. Hence, J_{ILM} has a positive sign if $C_{RET} > C_{VIT}$, i.e. if the drug molecules are moving from the retina to the vitreous humor; the sign will be negative otherwise. This is the reason why J_{ILM} has a negative contribution to the mass conservation equation in the retina (12) and a positive contribution to the mass conservation equation of the vitreous humor (13).

Following [27], the flux from the retina to the choroid through the retinal pigmented epithelium (RPE), J_{RPE}, is assumed to be proportional to the retinal concentration

$$J_{RPE} = S\, p_{RPE} \left(\frac{m_{RET}}{V_{RET}} \right) = S\, p_{RPE}\, C_{RET}, \tag{16}$$

assuming that the choroid is a sink.

The elimination flux from the vitreous humor to the aqueous humor J_{EL} is assumed to be proportional to the mass of drug in the vitreous humor, as follows

$$J_{EL} = \; k_{EL} m_{VIT} = k_{EL} C_{VIT} V_{VIT}, \tag{17}$$

where k_{EL} is the proportionality constant representing the vitreous humor elimination rate. Similarly, the clearance flux from the aqueous humor J_{CL} is assumed to be proportional to the mass of drug in the aqueous humor, as follows

$$J_{CL} = \; \frac{CL_{AQ}}{V_{AQ}} m_{AQ} = CL_{AQ} C_{AQ}, \tag{18}$$

where $\frac{CL_{AQ}}{V_{AQ}}$ is the proportionality constant representing the clearance from the aqueous humor per unit of volume. Note that, J_{RPE}, J_{EL}, and J_{CL} are unidirectional flows, while J_{ILM} is bidirectional.

Using the relation between mass and concentration, and using Eqs. (15)–(18), the conservation of mass Eqs. (12)–(14) can be rewritten fully in terms of the concentrations and are equivalent to Eqs. (1)–(3).

Appendix B: Model Solution and Numerical Approximation

We report here in detail the solution procedure used to solve Eqs. (1)–(3) with condition (4) or (5) and to obtain the results in Sect. 3.2. Equations (1)–(3) can be rewritten in the following vectorial/matrix form

$$\frac{d\vec{C}}{dt} = \boldsymbol{A}\,\vec{C} + \vec{F}\,, \tag{19}$$

where $\vec{C}\,(t) = \begin{bmatrix} C_{RET}(t) \\ C_{VIT}\,(t) \\ C_{AQ}\,(t) \end{bmatrix}$ is the vector of the unknown drug concentrations in each compartment at time t, $\vec{F}$ is the right-hand side vector, and $\boldsymbol{A}$ is the following coefficient matrix

$$\boldsymbol{A} = \begin{bmatrix} -\frac{S}{V_{RET}}\,(p_{RPE} + p_{ILM}) & \frac{S}{V_{RET}}\,p_{ILM} & 0 \\ \frac{S}{V_{VIT}}\,p_{ILM} & -\frac{S}{V_{VIT}}\,p_{ILM} - k_{EL} & 0 \\ 0 & k_{EL}\,\frac{V_{VIT}}{V_{AQ}} & -\frac{CL_{AQ}}{V_{AQ}} \end{bmatrix}. \tag{20}$$

Equation (19), can be solved analytically using the method of matrix exponential [39] and its solution is

$$\vec{C}\,(t) = \vec{C}_{\,0}e^{\boldsymbol{A}t} + \int_0^{\infty} e^{\boldsymbol{A}(t-s)}\vec{F}\,ds, \text{ where } e^{\boldsymbol{A}t} = \sum_{k=0}^{\infty}\frac{t^k}{k!}\boldsymbol{A}^k, \tag{21}$$

and $\vec{C}_{\,0} = \vec{C}\,(0)$ is the initial condition. In the intravitreal injection scenario, condition (4) can be rewritten as $\vec{C}_{\,0} = \begin{bmatrix} 0 \\ c_0 \\ 0 \end{bmatrix}$ and $\vec{F} = \vec{0}$. In the gene therapy scenario, condition (5) can be rewritten as $\vec{C}_{\,0} = \vec{0}$ and $\vec{F} = \begin{bmatrix} \frac{r}{V_{RET}} \\ 0 \\ 0 \end{bmatrix}$. To obtain the results in Sect. 3.2, we numerically approximate Eq. (21) by computing $e^{\boldsymbol{A}t}$ via the MATLAB algorithm *expm*, that uses a scaling and squaring algorithm with a Pade approximation, and by computing the integral in (21) via the Trapezoidal numerical integration *trapz* in MATLAB [31].

References

1. Friedman, DS, O'Colmain BJ, Munoz B, Tomany SC, McCarty C, De Jong P, Nemesure B, Mitchell P, Kempen J, Congdon N: Eye Diseases Prevalence Research Group. Prevalence of age-related macular degeneration in the United States. Arch Ophthalmol 122(4), 564–572 (2004).
2. Wong WL, Su X, Li X, Cheung CMG, Klein R, Cheung CY, Wong TY: Global prevalence of age-related macular degeneration and disease burden projection for 2020 and 2040: a systematic review and meta-analysis. Lancet Glob Health 2(2), e106–e116(2014).
3. Congdon N, O'Colmain B, Klaver CC, Klein R, Munoz B, Friedman DS, Kempen J, Taylor HR, Mitchell P, Hyman L: Eye Diseases Prevalence Research Group. Causes and prevalence of visual impairment among adults in the United States. Arch Opthamol 122, 477–485 (2004).
4. Guidoboni G, Harris A, Sacco R (Eds): Ocular Fluid Dynamics: Anatomy Physiology Imaging Techniques and Mathematical Modeling. Springer-Birkhäuser, New York (2019).
5. Jmarchn - Own work CC BY-SA 3.0 via Wikipedia Commons https://commons.wikimedia.org/w/index.php?curid=34828874.
6. Leung DW, Cachianes G, Kuang WJ, Goeddel DV, Ferrara N: Vascular endothelial growth factor is a secreted angiogenic mitogen. Science 246(4935), 1306–1309 (1989).
7. Ambati J, Ambati BK, Yoo SH, Ianchulev S, Adamis AP: Age-related macular degeneration: etiology, pathogenesis, and therapeutic strategies. Survey Ophthalmol. 48(3), 257–293 (2003).
8. Schwartz SG, Scott IU, Flynn Jr HW, Stewart MW: Drug delivery techniques for treating age-related macular degeneration. Expert Opin Drug Deliv 11(1), 61–8 (2014).
9. Flaxel CJ, Adelman RA, Bailey ST, Fawzi A, Lim JI, Vemulakonda GA, Ying GS: Age-related macular degeneration preferred practice pattern. Ophthalmol 127(1), 1–65 (2019).
10. Ruiz-Moreno JM, Arias L, Abraldes MJ, Montero J, Udaondo P: Economic burden of age-related macular degeneration in routine clinical practice: the RAMDEBURS study. Int Ophthalmol 41(10), 3427–36 (2021).
11. Singer MA, Awh CC, Sadda S, Freeman WR, Antoszyk AN, Wong P, Tuomi L: HORIZON: an open label extension trial of ranibizumab for choroidal neovascularization secondary to age-related macular degeneration. Ophthalmol 119(6), 1175–1183 (2012).
12. Rofagha S, Bhisitkul RB, Boyer DS, Sadda SV, Zhang K: SEVEN-UP Study Group. Seven-Year outcomes in Ranibizumab-Treated patients in anchor marina and horizon: a multicenter cohort study (seven-up). Ophthalmol 120(11): 2292–2299 (2013).
13. Heier JS, Brown DM, Chong V, Korobelnik JF, Kaiser PK, Nguyen QD, Kirchhof B, Ho A, Ogura Y, Yancopoulos GD, Stahl N, Vitti R, Berliner AJ, Soo Y, Anderesi M, Groetzbach G, Sommerauer B, Sandbrink R, Simader C, Schmidt-Erfurth U: Intravitreal aflibercept (VEGF trap-eye) in wet age-related macular degeneration. Ophthalmol 119(12), 2537–2548 (2012).
14. Brown DM, Michels M, Kaiser PK, Heier JS, Sy JP, Ianchulev T: Ranibizumab versus verteporfin photodynamic therapy for neovascular age-related macular degeneration: two-year results of the ANCHOR study. Ophthalmol 116(1), 57–65 (2009).
15. Rosenfeld PJ, Brown DM, Heier JS, Boyer DS, Kaiser PK, Chung CY, Kim RY: MARINA Study Group. Ranibizumab for neovascular age-related macular degeneration. N Engl J Med 355(14), 1419–1431 (2006).
16. Holz FG, Tadayoni R, Beatty S, Berger A, Cereda MG, Cortez R, Hoyng CB, Hykin P, Staurenghi G, Heldner S, Bogumil T, Heah T, Sivaprasad S: Multi-country real-life experience of anti-vascular endothelial growth factor therapy for wet age-related macular dege eration. Br J Ophthalmol 99, 220–226 (2015).
17. Ciulla TA, Huang F, Westby K, Williams DF, Zaveri S, Patel SC: Real-World outcomes of Anti–Vascular endothelial growth factor therapy in neovascular age-related macular degeneration in the United States. Ophthalmol Retina 2(7), 645–653 (2018).
18. Holekamp NM, Liu Y, Yeh W-S, Chia Y, Kiss S, Almony A, Kowalaski JW: Clinical utilization of anti-VEGF agents and disease monitoring in neovascular age-related macular degeneration. Am J Ophthalmol 157(4), 825–833 (2014).

19. Ciulla TA, Hussain RM, Pollack JS, Williams DF: Visual acuity outcomes and anti-vascular endothelial growth factor therapy intensity in neovascular age-related macular degeneration patients: A real-world analysis of 49485 eyes. Ophthalmol Retina 4(1), 19–30 (2020).
20. Rao P, Lum F, Wood K, Salman C, Burugapalli B, Hall R, Singh S, Parke II DW, Williams GA: Real-world vision in age-related macular degeneration patients treated with single anti-VEGF drug type for 1 year in the IRIS Registry. Ophthalmol 125(4), 522–528 (2018).
21. Avery RL, Campochiaro PA, Heier JS, Kiss S, Wykoff CC, Ho AC: The New Frontier: Gene Therapy for AMDClinical trials although in the earliest phases are showing exciting results. How might these treatments impact your practice in the future? Retina Today, May/June 2021 Features, https://retinatoday.com/articles/2021-may-june/the-new-frontier-gene-therapy-for-amd, last accessed 2022/05/21.
22. Friedrich S, Cheng YL, Saville B: Finite element modeling of drug distribution in the vitreous humor of the rabbit eye. Ann Biomed Eng 2, 303-14 (1997).
23. Missel PJ. Simulating intravitreal injections in anatomically accurate models for rabbit monkey and human eyes. Pharm Res 29(12), 3251–72 (2012).
24. Zhang Y, Bazzazi H, de Silva RL, Pandey NB, Green JJ, Campochiaro PA, Popel AS: Three-dimensional transport model for Intravitreal and Suprachoroidal drug injection. Invest Ophthalmol Vis Sci 159(12), 5266–76 (2018).
25. Xu L, Lu T, Tuomi L, Jumbe N, Lu J, Eppler S, Kuebler P, Damico-Beyer LA, Joshi A: Pharmacokinetics of ranibizumab in patients with neovascular age-related macular degeneration: a population approach. Invest Ophthalmol Vis Sci 154(3), 1616–24 (2013).
26. Hutton-Smith LA, Gaffney EA, Byrne HM, Maini PK, Schwab D, Mazer NA: A mechanistic model of the intravitreal pharmacokinetics of large molecules and the pharmacodynamic suppression of ocular vascular endothelial growth factor levels by ranibizumab in patients with neovascular age-related macular degeneration. Mol Pharm 13(9), 2941–50 (2016).
27. Hutton-Smith LA, Gaffney EA, Byrne HM, Maini PK, Gadkar K, Mazer NA: Ocular pharmacokinetics of therapeutic antibodies given by intravitreal injection: estimation of retinal permeabilities using a 3-compartment semi-mechanistic model. Mol Pharm 714(8), 2690–6 (2017).
28. Ahn SJ, Hong HK, Na YM, Park SJ, Ahn J, Oh J, Chung JY, Park KH, Woo SJ: Use of rabbit eyes in pharmacokinetic studies of intraocular drugs. J Vis Exp 23(113), e53878 (2016).
29. Brubaker RF: Flow of aqueous humor in humans [The Friedenwald Lecture]. Invest Ophthalmol Vis Sci 132(13), 3145–66 (1991).
30. Krohne TU, Liu Z, Holz FG, Meyer CH: Intraocular pharmacokinetics of ranibizumab following a single intravitreal injection in humans. Am J Ophthalmol 1154(4), 682–6 (2012).
31. MATLAB and Optimization Toolbox Release 2021b, The MathWorks Inc. Natick Massachusetts United States.
32. Ranibizumab intravitreal injection (Rx), https://reference.medscape.com/drug/lucentis-byooviz-ranibizumab-intravitreal-injection-343645, last accessed 2022/05/21.
33. Heier J: Key Takeaways from the RGX-314 Phase I/IIa Clinical Trial for Wet AMD (Cohorts 1-5), AAO Retina Subspecialty Days 2019/10/11, https://regenxbio.com/wp-content/uploads/2019/10/Key-Takeaways-From-The-RGX-314-Phase-I-IIa-Clinical-Trial-For-Wet-AMD-Cohorts-1-5.pdf, last accessed 2022/05/21.
34. Safety and Tolerability of RGX-314 Gene Therapy for Neovascular AMD Trial, https://clinicaltrials.gov/ct2/show/NCT03066258, last accessed 2022/05/21.
35. Avery R: Two Year Results from the Subretinal RGX-314 Gene Therapy Phase 1/2a Study for the Treatment of Neovascular AMD, and an Update on Suprachoroidal Trials, AAO Retina Subspecialty Day 2021/11/12, https://www.regenxbio.com/wp-content/uploads/2022/01/RGX-314_BobAvery-AAO-2021_11Nov21_FINAL.pdf, last accessed 2022/05/21.
36. Singh RP, Kaiser PK: Role of ranibizumab in management of macular degeneration. Indian J Ophthalmol 55(6), 421 (2007).
37. Lowe J, Araujo J, Yang J, Reich M, Oldendorp A, Shiu V, Quarmby V, Lowman H, Lien S, Gaudreault J, Maia M: Ranibizumab inhibits multiple forms of biologically active vascular endothelial growth factor in vitro and in vivo. Expe Eye Res 85(4), 425–30 (2007).

38. Ding K, Shen J, Hafiz Z, Hackett SF, de Silva RL, Khan M, Lorenc VE, Chen D, Chadha R, Zhang M, Van Everen S: AAV8-vectored suprachoroidal gene transfer produces widespread ocular transgene expression. J Clin Investig 1129(11), 4901–11 (2019).
39. Chicone C: Ordinary Differential Equations with Applications. Texts in Applied Mathematics, Springer (2006).